# Accelerated orbital decay of supermassive black hole binaries in merging nuclear star clusters

G. Ogiya, Oliver Hahn, Chiara M.F. Mingarelli, Marta Volonteri

Monthly Notices
of the
ROYAL ASTRONOMICAL SOCIETY

MNRAS **493,** 3676–3689 (2020)
Advance Access publication 2020 February 13

doi:10.1093/mnras/staa444

# Accelerated orbital decay of supermassive black hole binaries in merging nuclear star clusters

Go Ogiya [1,2,3]★ Oliver Hahn [1] Chiara M. F. Mingarelli [4,5] and Marta Volonteri[6]

[1] *Observatoire de la Côte d'Azur, CNRS, Boulevard de l'Observatoire, Laboratoire Lagrange, Université Côte d'Azur, CS 34229, F-06304 Nice, France*
[2] *Waterloo Centre for Astrophysics, University of Waterloo, Waterloo, ON N2L 3G1, Canada*
[3] *Department of Physics and Astronomy, University of Waterloo, 200 University Avenue West, Waterloo, ON N2L 3G1, Canada*
[4] *Center for Computational Astrophysics, Flatiron Institute, 162 Fifth Avenue, New York, NY 10010, USA*
[5] *Department of Physics, University of Connecticut, 196 Auditorium Road, U-3046, Storrs, CT 06269-3046, USA*
[6] *Institut d'Astrophysique de Paris, Sorbonne Université, UPMC Univ CNRS, UMR 7095, 98 bis Boulevard Arago, F-75014 Paris, France*

Accepted 2020 February 11. Received 2020 January 20; in original form 2019 October 18

## ABSTRACT

The coalescence of supermassive black holes (SMBHs) should generate the strongest sources of gravitational waves (GWs) in the Universe. However, the dynamics of their coalescence is the subject of much debate. In this study, we use a suite of *N*-body simulations to follow the merger of two nuclear star clusters (NSCs), each hosting an SMBH in their centre. We find that the presence of distinct star clusters around each SMBH has important consequences for the dynamical evolution of the SMBH binary: (i) The separation between the SMBHs decreases by a few orders of magnitude in the first few Myrs by the combined effects of dynamical friction and a drag force caused by tidally stripped stars. In fact, this is a significant speedup for equal mass ratio binaries, and becomes extreme for unequal mass ratios, e.g. 1:10 or 1:100, which traditional dynamical friction alone would not permit to bind. (ii) The subsequent binary hardening is driven by the gravitational slingshots between the SMBH binary and stars, and also depends on the mass ratio between the SMBHs. Thus, with this additional drag force, we find that all SMBHs in our suite coalesce within a Hubble time. Given that about 50 per cent of Milky Way-sized galaxies host NSCs, our results are encouraging for upcoming GW observations with the Laser Interferometer Space Antenna – LISA – which will detect SMBH coalescence in the $10^4$–$10^7$ $M_\odot$ mass range.

**Key words:** black hole physics – gravitational waves – methods: numerical – galaxies: kinematics and dynamics – galaxies: star clusters: general.

## 1 INTRODUCTION

The detection of gravitational waves (GWs) by the advanced Laser Interferometer Gravitational-Wave Observatory (aLIGO) and Virgo helped to establish a new field of astronomy (Abbott et al. 2016, and subsequent detections). Thus far, high-frequency GWs have been detected from merging stellar mass black holes (BHs) and neutron stars. The binary masses of the detected events range from ∼3 to ∼60 $M_\odot$, which while interesting, will be dwarfed by supermassive massive black hole (SMBH) coalescence in the centres of galaxies. In the next decade, the low-frequency inspiral of the most massive SMBH binaries (SMBHBs), $\gtrsim 10^8$ $M_\odot$, is expected to be detected by pulsar timing arrays (PTA; Mingarelli et al. 2017; Kelley et al. 2018), while the final coalescence of SMBHs in the $10^4$–$10^7$ $M_\odot$ range will be accessible with the upcoming Laser Interferometer Space Antenna (LISA; Amaro-Seoane et al. 2017), and is the subject of our study here.

A likely formation channel of SMBHBs is through galaxy mergers, ubiquitously observed and expected by the standard paradigm of hierarchical structure formation in the Universe. After a galaxy merger, the SMBHs are expected to experience the following three phases before emitting GWs (Merritt 2013). In the first stage (pre-binary phase), dynamical friction of stars and dark matter (e.g. Chandrasekhar 1943; Antonini & Merritt 2012; Ogiya & Burkert 2016) as well as of the interstellar gas (e.g. Ostriker 1999; Escala et al. 2004; Tanaka & Haiman 2009) plays a role in depleting the SMBH's angular momentum and orbital energy with respect to the centre of the merged galaxy. The SMBHs therefore sink towards the centre of the merged galaxy, and the separation between them, $d$, decreases. When $d$ falls below the gravitational influence radius of the more massive (primary) BH,

$$d_{\rm b} \equiv \frac{GM_1}{\sigma^2}, \tag{1}$$

the SMBHs form a bound binary. Here, $G$ is the gravitational constant and $M_1$ and $\sigma$ are the mass of the primary SMBH and velocity dispersion of stars, respectively. When the merged galaxy

★ E-mail: gogiya@uwaterloo.ca

is in a virial equilibrium state, $d_{\rm b}$ roughly corresponds to the radius of a sphere enclosing a stellar mass of $2M_1$.

The SMBHB then experiences a rapid orbital decay driven by the combined effects of dynamical friction and gravitational slingshots between the SMBHB and stars (combined effect phase). While this phase lasts only for a short time, $\lesssim 10\,\tau$, where $\tau$ is the *N*-body or Hénon time unit (Hénon 1971; Heggie 2014), $d$ decreases by one to two orders of magnitude (Milosavljević & Merritt 2001; Merritt 2006).

When the specific negative binding energy of the binary exceeds the typical specific negative binding energy of stars, $\sigma^2$, the SMBHB proceeds to the hard binary phase. This condition translates to $d$ being below the hard binary separation, i.e.

$$d_{\rm hb} \equiv \frac{G\mu}{4\sigma^2} = \frac{M_2}{M_1+M_2}\frac{d_{\rm b}}{4}, \tag{2}$$

where $M_2$ is the mass of the second SMBH ($M_2 \leq M_1$) and $\mu \equiv M_1M_2/(M_1+M_2)$ is the reduced mass of the SMBHB. While the exact definition of the hard binary separation depends on literature, we adopt equation (2) in this paper. In this phase, the motion of the two SMBHs is almost purely Keplerian.

Even after reaching $d_{\rm hb}$, stars interacting with the SMBHB can extract orbital energy and angular momentum from it, so that the orbit can in principle continue to decay, although there is some debate surrounding this issue. Indeed, if not enough SMBHB-star scattering occurs during the hard binary phase, the binary stalls before it reaches the GW-emission phase – the infamous final parsec problem. For example, in spherical systems without gas, the orbital decay of the SMBHB stops because of a deficit of low orbital energy, and angular momentum stars and dark matter to interact with the SMBHB, the so-called loss cone depletion (Begelman, Blandford & Rees 1980; Milosavljević & Merritt 2003). A number of solutions have been proposed to the final parsec problem, e.g. the importance of a non-spherical galactic potential (Berczik et al. 2006; Khan et al. 2013; Vasiliev, Antonini & Merritt 2015; Gualandris et al. 2017), which suggest that the hardening rate could be close to what is expected in the full loss cone regime (Sesana & Khan 2015). Viscous interactions in circumbinary discs (Escala et al. 2005; Cuadra et al. 2009; Lupi et al. 2015; Tagawa et al. 2015) are also relevant in the case of a gas-dominated nucleus, although simulations have been finding conflicting results on the sign of the torque, i.e. whether the interaction between the binary and the gas shrinks the binary separation (negative torque), or increases it (positive torque) (Moody, Shi & Stone 2019, and references therein). Further interactions with SMBHs from subsequent galaxy mergers have also been shown to lead to their coalescence (Iwasawa, Funato & Makino 2006; Tanikawa & Umemura 2011; Bonetti et al. 2018; Ryu et al. 2018), mostly when high eccentricities are excited through the Kozai–Lidov mechanism (Kozai 1962; Lidov 1962).

Nuclear star clusters (NSCs) – dense stellar systems with mass density of $\rho \gtrsim 10^6\,{\rm M}_\odot\,{\rm pc}^{-3}$, and of order $\mathcal{O}$(pc) across (e.g. Sánchez-Janssen et al. 2019, and references therein) – may be among the most important factors in the evolution of SMBHs in the LISA band for GW observations. The masses of NSCs appear to correlate with the mass of their host galaxies (Georgiev et al. 2016; Sánchez-Janssen et al. 2019, and references therein). Sánchez-Janssen et al. (2019) showed that their presence in galaxies depends on the galaxy's stellar mass, $M_{\rm gal}$, and peaks at $M_{\rm gal} \approx 10^9\,{\rm M}_\odot$, where up to 90 per cent of galaxies appear to host an NSC, while the fraction drops below 20 per cent at $M_{\rm gal} \approx 10^7\,{\rm M}_\odot$ and $M_{\rm gal} \approx 10^{11}\,{\rm M}_\odot$. An NSC and an SMBH co-exist in the centre of many galaxies, even locally, in the centre of our Milky Way (Schödel et al. 2007; Ghez et al. 2008; Gillessen et al. 2009; Genzel, Eisenhauer & Gillessen 2010). Assuming that all NSCs host an SMBH in their centre, about 50 per cent of Milky Way-sized galaxies should host both an NSC and an SMBH in their centre. In addition, numerical simulations of SMBHB formation through galaxy mergers find that gas compression triggers bursts of star formation at pericentres. As a result, dense NSCs are formed and the SMBHs are embedded in them (Van Wassenhove et al. 2014) during the last phase of the galaxy merger. Furthermore, recent searches for SMBHs in dwarf galaxies have successfully found them (Nguyen et al. 2018), and classic analytic estimates of the SMBHB hardening time-scales suggest a more rapid evolution than expected in dwarf galaxies in the presence of NSCs due to the increased stellar densities (Biava et al. 2019).

Note that the contribution of NSCs to the orbital evolution of SMBHs in the PTA band (corresponding to $\gtrsim 10^8\,{\rm M}_\odot$) would be subdominant because the mass of NSCs is not large enough with respect to the SMBH mass. Therefore, we restrict our discussion in this paper to the orbital evolution of SMBHs in the LISA band.

Here, we show that tidal effects from the merging NSCs accelerate the orbital evolution time-scale of SMBHs before and around the time the binary is formed. In the presence of NSCs the formation of a hard binary occurs faster, accelerating the *whole* process of orbital decay into the GW regime. Using a suite of *N*-body simulations, we find that the relative orbit can be further efficiently shrunk by the interactions with NSC stars at the spatial scale of $\ll$ pc, helping the binary to overcome the final parsec problem. Therefore, NSCs appear to be an important ingredient in accelerating the coalescence of SMBHBs.

This paper is organized as follows. The role of tidally stripped stars in the orbital evolution of merging NSCs is discussed with a simple analytical model in Section 2. We describe the simulation setup in Section 3 and explore the simulation results in Section 4. In Section 5, we discuss implications for GW observations before summarizing the paper in Section 6.

## 2 EFFECTIVE DRAG FORCE BY STRIPPED STARS

In this section, we discuss how stars which were tidally stripped from their NSC can shrink an SMBHB's orbit. Let us consider that two NSCs each hosting an SMBH are orbiting each other. Stars in the outskirts of NSCs are less bound compared to those in the centres, and hence they are more easily affected by the tidal force of the other NSC. As a result, stars in the outskirts are exchanged between the NSCs or may become unbound if their orbital energy and/or angular momentum have been changed during the tidal interaction.

Huang (1963, see also Huang 1956) investigated the orbital evolution of binary systems which can exchange and/or eject mass, and found that when the ejected mass reaches a distance larger than the semimajor axis of the binary, angular momentum of the binary can be carried away and the binary orbit shrinks. While they discussed the orbital evolution of binary stars via an analytical model, it is quite general and applicable for the cases we study.

We begin with a brief overview of the Huang (1963) model. Specific angular momentum of stars in the NSC binary system and its mass are, respectively, denoted as $l$ and $m$. The change in $l$ through the mass-loss event is

$$\delta l = (l_{\rm s} - l)\frac{\delta m_{\rm s}}{m}, \tag{3}$$

where the subscript 's' represent quantities of stripped stars. For simplicity, we suppose $\delta m_s < 0$ and $|\delta m_s| \ll m$ and that the eccentricity, $e$, of stripped stars is not changed. The latter assumption should be valid until the stripped stars arrive at peri- or apocentre where they can be mixed effectively and thus for about an orbital period, i.e. the mixing period of the tidally stropped stars is comparable to the NSC orbital period. Then the specific angular momentum of each component is given as

$$l = \sqrt{Gma(1-e^2)} \tag{4}$$

$$l_s = \sqrt{Gm(a+\delta a)(1-e^2)} \tag{5}$$

where $a$ and $a + \delta a$ are the semimajor axis of the NSC binary and the typical semimajor axis of stripped stars, respectively. Because $\delta m_s < 0$, the condition to lose specific angular momentum by tidal stripping, $\delta l < 0$, is

$$\delta a > 0. \tag{6}$$

The exchange of angular momentum during the NSC merger process leads to an expansion of the orbit of the stripped stars. This in turn reduces the angular momentum of the NSC binary leading to orbital decay of their central SMBHs. The tidally stripped material thus exerts a net drag force on to the binary (e.g. Fujii, Funato & Makino 2006; Fellhauer & Lin 2007; van den Bosch & Ogiya 2018; Ogiya et al. 2019).

As we show in Section 4, the model by Huang (1963) is a macroscopic description for the rapid orbital decay of SMBHs. The more microscopic description we find in Section 4 is that the leading arm of the NSC attaches to and decelerates the companion NSC's SMBH, so that the binary NSCs appear like a pair of snakes biting each other's tail. Hereafter, we refer to this type of drag force as the ouroboros effect, shown in Fig. 1.

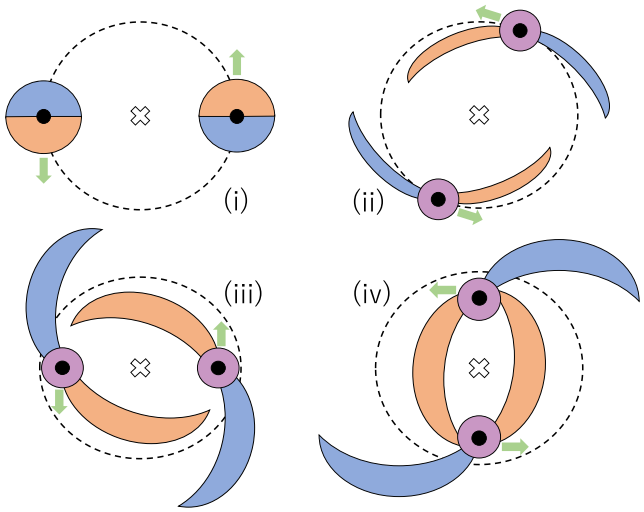


**Figure 1.** Concept of the ouroboros effect. Time evolution is illustrated in four panels. Initially, two NSCs each hosting an SMBH (black circle) at the centre are orbiting anticlockwise. The cross and dashed circle are the centre of mass of the entire system and initial relative orbit of the SMBHs. (i) Stars on the downstream (red) are decelerated by their own SMBH and stars on the upstream side (blue). As a backreaction, stars on the upstream side are accelerated. (ii) Because of the tidal force of the other NSC, the stars on the downstream and upstream sides form a leading arm and trailing tail, respectively, while stars in the centre of the NSC surround the SMBH since they are tightly bound and resilient to the tidal force (purple). (iii) The leading arm and trailing tail grow with time. Because the leading arm (trailing tail) consists of the decelerated (accelerated stars), its orbit is shrunk (expanded). (iv) The leading arm gets close to the SMBH of the other NSC and decelerates it. The two leading arms are like a pair of snakes biting each other's tail (SMBH). We describe this process in more detail in Section 4.1.

## 3 SIMULATION SET-UP

We perform a suite of two types of collisional $N$-body simulations to investigate the orbital evolution of SMBHs in the presence of NSCs. The first type of simulation (type-M, for 'merging') follows mergers between two NSCs, each containing an SMBH in its centre, a situation that is expected to ensue after a major galaxy merger (mass ratio $\geq$1:4, Van Wassenhove et al. 2014). In these simulations both the ouroboros effect and dynamical friction are at play. In the second type of simulation (type-O, for 'orbiting'), we consider a scenario where the primary SMBH is located at the centre of its NSC, and the second SMBH is orbiting this primary system without an NSC of its own. In this case, only dynamical friction is at work. Type-O simulations thus represent astrophysical cases where the second galaxy has been completely disrupted (typically in minor galaxy mergers with mass ratio <1:4), when an SMBH returns after an ejection, e.g. through a three-body interaction or a GW kick (e.g. Volonteri & Perna 2005), or when NSCs are formed through mergers between globular clusters hosting massive BHs in each (Antonini et al. 2012; Mastrobuono-Battisti, Perets & Loeb 2014; Arca-Sedda & Gualandris 2018).

### 3.1 Density profile of NSCs and merger set-up

For the NSCs, we model their initial density distribution using the spherical profile by Dehnen (1993)

$$\rho(r) = \frac{(3-\gamma)M_{\rm nsc,tot}}{4\pi}\frac{r_0}{r^\gamma(r+r_0)^{4-\gamma}}, \tag{7}$$

where $r$, $r_0$, and $M_{\rm nsc,\,tot}$ represent the distance from the centre, core size, and total stellar mass of the NSC, respectively. In all simulations, we assume a centrally cored profile, $\gamma = 0$, and set the core size as $r_0 = 1.4$ pc which leads to an effective radius of 4 pc, consistent with the observations of NSCs with mass of $\approx 10^7\,{\rm M}_\odot$ (Georgiev et al. 2016). NSCs may actually have steeper density slopes producing a higher central density. For example, the density structure of the Milky Way's NSC is modelled with $\gamma = 0.5$ (Chatzopoulos et al. 2015). If the central density is higher, interactions between SMBHs and stars would be more frequent: the orbital decay rate in our simulations therefore represents a lower limit.

In the type-M simulations, each NSC has a stellar mass of $M_{\rm nsc,\,tot} = 10^7\,{\rm M}_\odot$. The NSC in type-O simulations has a stellar mass of $M_{\rm nsc,\,tot} = 2 \times 10^7\,{\rm M}_\odot$ so that the total stellar mass is the same in both simulations. We fix the mass of the primary SMBH to be $M_1 = 10^6\,{\rm M}_\odot$, and vary that of the second, $M_2$, motivated by the scatter of BH mass in NSCs (Georgiev et al. 2016). We define the mass ratio between the SMBHs as

$$q \equiv M_2/M_1. \tag{8}$$

In the type-M simulations, each NSC consists of 65 536 equal mass stellar particles and one SMBH particle, so that the total number of particles in a simulation is 131 074. In type-O simulations, the NSC has 131 072 equal mass stellar particles and two SMBH particles are included so that the total number of particles is also 131 074. In both models, the mass of the stellar $N$-body particles is $\approx$152.6 $\,{\rm M}_\odot$. We draw the position vector of stellar particles by

rejection sampling based on the density profile. Then, an SMBH is placed at the centre of the NSC with zero velocity with respect to the cluster centre. The velocity vectors of the stellar particles are drawn as follows to ensure that the NSC is in equilibrium. Assuming that the initial velocity structure of the NSC is isotropic, we can employ the Eddington formula (Eddington 1916) to obtain the phase-space distribution function from the density profile. The central SMBH must of course also be taken into account to compute the gravitational potential. Then, we draw for each particle an isotropic unit vector and multiply it with a velocity magnitude obtained by rejection sampling from the distribution function at the particle position. We verify that the NSC model with the central SMBH is reasonably stable in isolation (Appendix A) for time-scales much longer than those relevant for the physical processes we analyse in this paper.

We denote the initial separation between two SMBHs as $d_{\rm i}$.[1] To characterize the initial relative velocity between two SMBHs,[2] we introduce another parameter that characterizes the angular momentum of the orbit, $\eta$, and take only the stellar mass into account. The mass of the merging systems is taken to be $M_*(d_{\rm i}) \equiv \sum_{n=1}^{2} M_{\rm nsc}(< d_{\rm i}/2) = 2M_{\rm nsc}(< d_{\rm i}/2)$, where $M_{\rm nsc}(< r)$ is the stellar mass enclosed within $r$ from the centre of the NSC with a total mass of $10^7$ M$_\odot$. The initial relative velocity, $v_{\rm i}$, is evaluated as

$$v_{\rm i} = \eta \sqrt{\frac{G M_*(d_{\rm i})}{d_{\rm i}}}. \tag{9}$$

The primary SMBH is initially set at the origin with zero-velocity and the position and velocity vectors of the second SMBH are $\mathbf{X} = (d_{\rm i}, 0, 0)$ and $\mathbf{V} = (0, v_{\rm i}, 0)$, respectively. Note that two SMBHs are initially at the apocentre of the relative orbit and the second SMBH initially has the same specific angular momentum with respect to the primary SMBH in the simulations with the same $d_{\rm i}$ and $\eta$, i.e. the $Z$-component of the initial specific angular momentum vector is given as $\bar{L}_{\rm z} = \eta\sqrt{G M_*(d_{\rm i}) d_{\rm i}}$.

The setups of type-O and -M simulations are similar to those in Merritt (2006) and Preto et al. (2011), respectively. The simulations by Merritt (2006) studied the orbital evolution of SMBHBs in a galactic nucleus, hosting the primary SMBH at the centre and the second SMBH is orbiting in the nucleus. Indeed, Merritt (2006) showed that the time-scale of orbital decay due to dynamical friction depends on the mass of the second SMBH, as expected from Chandrasekhar's theory (Chandrasekhar 1943). Preto et al. (2011) studied the orbital decay of SMBHBs in the non-spherical gravitational potential field caused by a merger between two NSCs. While they varied the mass ratio between the NSC and SMBH, the two SMBHs had the same mass, i.e. $q = 1.0$. Motivated by observations that indicate significant scatter in the mass of SMBHs at a fixed NSC mass scale (Georgiev et al. 2016), we vary the mass of the second SMBH, $M_2$, fixing $M_1$ as well as $M_{\rm nsc,\,tot}$, so that type-M simulations are complementary to simulations by Preto et al. (2011). Table 1 provides a summary of parameters adopted in the simulations. The initial separation between SMBHs, $d_{\rm i} = 20$ or 50 pc, is larger than the effective radius of the NSC model (4 pc) and large enough to prevent the SMBHs from being bound to each other initially.

Finally, we note that we do not consider here additional possible sophistications, such as non-monochromatic stellar mass functions and associated mass segregation in the NSCs. Especially the latter might play an important role by keeping more massive stars more tightly bound to the central SMBHs.

[1] In type-M simulations, $d_{\rm i}$ corresponds to the initial separation between the centres of two NSCs.

[2] This corresponds to the initial relative bulk velocity between two NSCs in type-M simulations.

**Table 1.** Summary of the simulation parameters. Column (1) Type of simulation. Type-M simulates a merger between two NSCs, hosting an SMBH in each centre. In type-O, the primary SMBH is settled in the centre and the second one is initially orbiting in the NSC. (2) Mass ratio between two SMBHs. The mass of the primary SMBH is $10^6$ M$_\odot$ in all simulations. (3) Initial separation between SMBHs in pc. (4) Parameter to control the initial angular momentum. (5) $N$-body time unit in Myr.

| (1) Run type | (2) $q$ | (3) $d_{\rm i}$ | (4) $\eta$ | (5) $\tau$ (Myr) |
|---|---|---|---|---|
| M | 0.01 | 20 | 1.0 | 0.102 |
| M | 0.1 | 20 | 0.5 | 0.084 |
| M | 0.1 | 20 | 1.0 | 0.101 |
| M | 0.1 | 50 | 1.0 | 0.127 |
| M | 1.0 | 20 | 1.0 | 0.088 |
| O | 0.01 | 20 | 1.0 | 0.054 |
| O | 0.1 | 20 | 0.5 | 0.054 |
| O | 0.1 | 20 | 1.0 | 0.054 |
| O | 0.1 | 50 | 1.0 | 0.055 |
| O | 1.0 | 20 | 1.0 | 0.058 |

### 3.2 Simulation code

Both the ouroboros effect and dynamical friction are *collisionless* processes since they are caused by the change in the distribution of bulk of stars, not by encounters with single stars. However, to investigate the dynamics of SMBHs in dense NSCs, especially after SMBHs form a tightly bound hard binary ($d < d_{\rm bh}$), it is important to properly handle the collisional nature of the system in order to capture the hardening through stellar scattering.

There are difficulties in solving collisional dynamics in numerical simulations, such as the requirement of accurate time integration in close encounter events, and computational expensiveness. A well-established $N$-body simulation code for collisional dynamics, NBODY6 (Aarseth 2003), includes key algorithms and mathematical sophistication such as block time-steps (McMillan 1986; Makino 1991), splitting the total force into two parts, a slowly changing part from distant particles (regular force) and local contribution changing in a shorter time-scale (irregular force), based on neighbour scheme by Ahmad & Cohen (1973), and the Kustaanheimo–Stiefel (KS) regularization algorithms by Kustaanheimo & Stiefel (1965, see also e.g. Saha 2009) and by Mikkola & Aarseth (1993), to overcome the numerical difficulties. NBODY6 has been accelerated by parallelization, graphic processing units (GPUs) and single instruction multiple data (SIMD) procedures (Nitadori & Aarseth 2012, see also e.g. Tanikawa et al. 2012). Here, we use the latest descendant, NBODY6++GPU[3] (Wang et al. 2015), for our calculations.

NBODY6++GPU has several parameters controlling the accuracy of orbit integration. The parameters determining the time-steps for the regular and irregular forces, $\eta_{\rm r}$ and $\eta_{\rm i}$, and for the KS regularization, $\eta_{\rm u}$, are 0.005, 0.005, and 0.05, respectively. In Appendix B, we show that smaller $\eta_{\rm r}$, $\eta_{\rm i}$, and $\eta_{\rm u}$ (i.e. smaller time-steps) lead to better energy conservation (but still comparable to that in the simulation with the fiducial parameter set) while the orbital evolution of the SMBHB is almost independent of them. The time-step and distance criteria for regularization search, d$t_{\rm min}$ and

[3] https://github.com/nbodyx/Nbody6ppGPU

$r_{\rm min}$, and the energy criterion to distinguish soft binaries from hard binaries, $E_{\rm close}$, are initially $2 \times 10^{-6}$, $5 \times 10^{-4}$, and 1, and adjusted every 0.01 $\tau$, based on the definition of close encounters (deflection of 90 deg). The maximum number of KS regularization pairs (star–star or SMBH-star) at the same time is a few in each simulation.

The number of neighbour particles, $N_{\rm nbopt}$, determines the size of the sphere containing neighbour particles that cause the irregular force. A larger $N_{\rm nbopt}$ leads to a larger neighbour sphere and is expected to yield higher force accuracy while the numerical cost increases. We adopt $N_{\rm nbopt} = 64$ and have a relative energy conservation of ∼one per cent at the end of simulations ($t = 20$ Myr). In Appendix B, we show that the energy conservation and the orbital evolution of the SMBHB is almost independent of $N_{\rm nbopt}$.

Collisionality of the simulated systems can still be higher than in reality because the number of stellar particles is less than that of stars in NSCs. If the average mass of stars is 1 $M_\odot$, an NSC with a mass of $10^7$ $M_\odot$ would contain $10^7$ stars. To investigate the importance of collisionality in the orbital evolution of the SMBHs, we also perform a collisionless $N$-body simulation and find that the results of collisional and collisionless simulations agree with each other when the traditional dynamical friction and the ouroboros effect play a key role (Appendix C). We also note that the collisional simulation results are insensitive to the number of stellar particles, i.e. mass resolution (see Fig. 6).

## 4 SIMULATION RESULTS

### 4.1 Ouroboros effect

Here, we investigate how the ouroboros effect arises. The left-hand panels of Fig. 2 illustrate the distribution of stellar particles in the type-M simulation of $q = 0.1$, $d_{\rm i} = 20$ pc, and $\eta = 1.0$. The positions of the primary and secondary SMBHs are shown as a circle and a cross. While the central parts of the two NSCs are initially separated by 20 pc, the distance between them rapidly decreases ($\lesssim 1$ pc at $t = 1.5$ Myr). The time-scale of orbital decay by dynamical friction is expected to be >10 Myr (see Section 4.2), so other mechanisms must be in play to drive the rapid orbital decay shown in Fig. 2.

To understand how the separation between the SMBHs decreases in such a short time, we analyse the distribution of stellar particles based on the $Z$-component of the angular momentum vector of each particle, $L_z$, since the initial bulk motion of the merging NSCs is anticlockwise on the $XY$ plane with no bulk motion in the $Z$-direction. The right-hand panels of Fig. 2 demonstrate that upstream and downstream particles gain and lose $L_z$. This is because the upstream particles are pulled by the NCS core, the SMBH and central stars, while the downstream ones pull the NSC core. This divide particles into two populations, gaining and losing angular momentum. Particles losing $L_z$ (white) fall towards the centre of the merging system, i.e. potential minimum, and particles gaining $L_z$ (black) are distributed outside.

In Fig. 3, we study the mechanism of the rapid orbital decay from a macro perspective, based on the model by Huang (1963, a brief review is given in Section 2). We track some features of stellar particles that gain (black solid) and lose (red dotted) $L_z$ during the dynamical evolution of the NSC merger in the M-type simulation with $q = 0.1$, $d_{\rm i} = 20$ pc, and $\eta = 1.0$. The upper panel shows that the mass of the population gaining $L_z$ is comparable to that of the population losing $L_z$ and does not significantly change with time. The lower panel presents the averaged change in the distance between the centre of mass of the entire system and stellar particles that belong to each population. We find that the population gaining

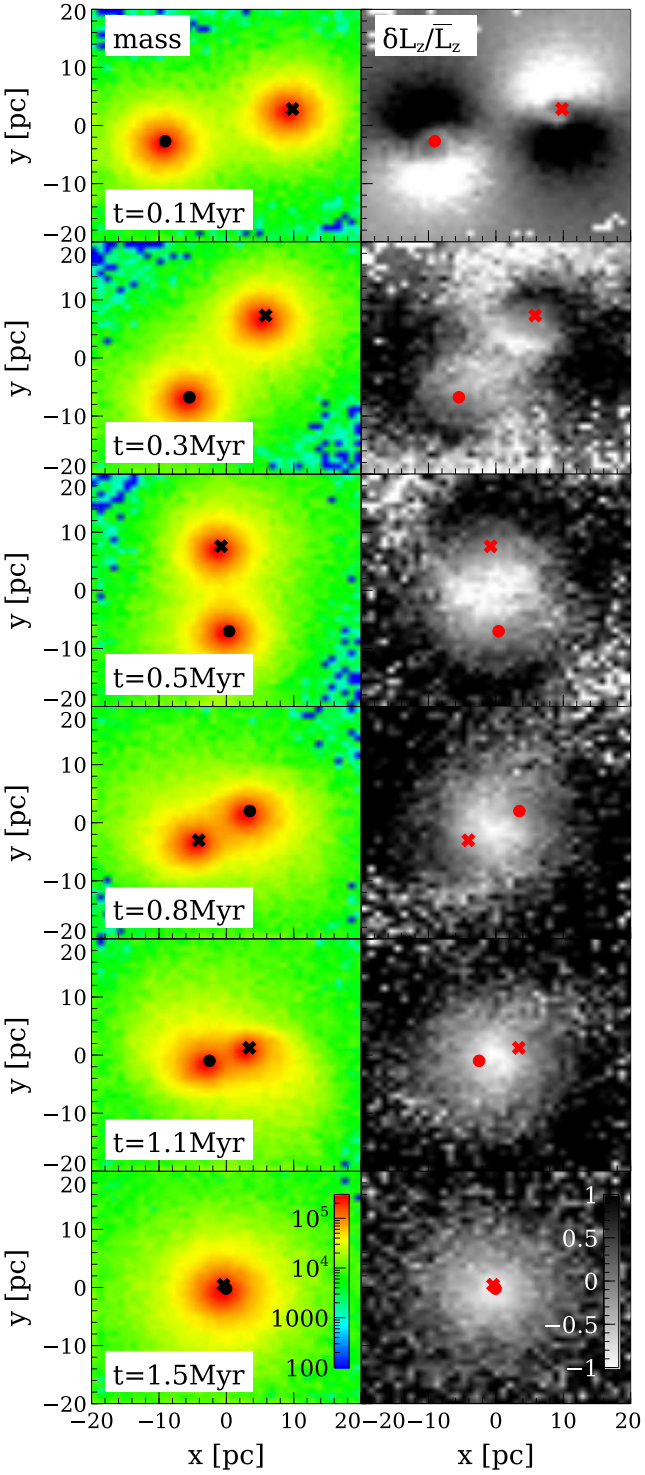


**Figure 2.** (*Left*) Stellar mass distribution projected on the $XY$-plane (in $M_\odot$). (*Right*) Change in the $Z$-component of the angular momentum vector of each particle, $\delta L_z$, scaled by that of the initial bulk motion of the entire system, $\bar{L}_z$. Stellar particles in the range of $Z = [-10: 10]$ pc are taken into account. The origin corresponds to the centre of mass of the entire system in the type-M simulation of $q = 0.1$, $d_{\rm i} = 20$ pc, and $\eta = 1.0$. A circle and a cross represent primary and secondary SMBHs, respectively. Time evolution is demonstrated from top to bottom. The distance between the SMBHs is reduced to <1 pc in the first few Myr.

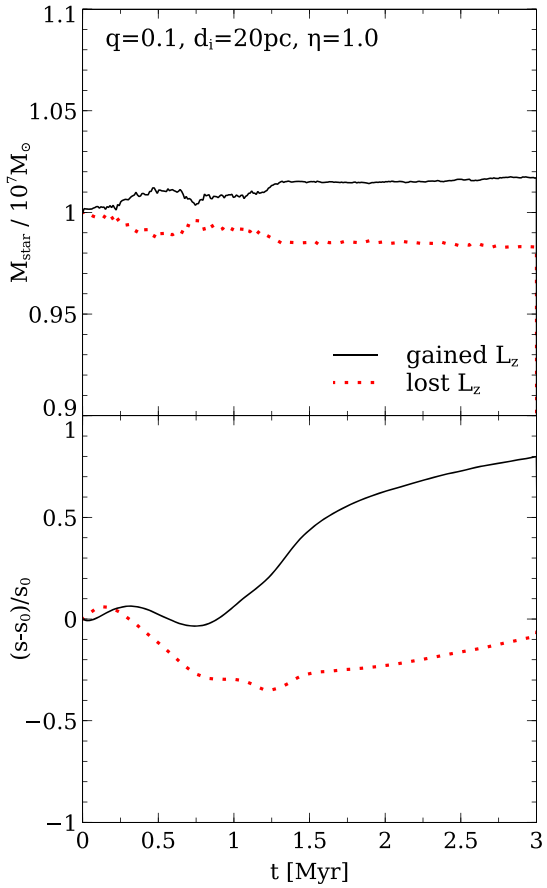


**Figure 3.** Evolution of stellar particles gaining (black solid) and losing $L_z$ (red dotted) in the type-M simulation of $q = 0.1$, $d_i = 20$ pc, and $\eta = 1.0$. (*Upper*) Mass of each population. (*Lower*) Change in the distance to the centre of mass of the merged system, $s$. The subscript of '0' represents the initial value. The orbits of stars gaining $L_z$ expand while those of stars losing $L_z$ shrink, consistent with the model by Huang (1963).

$L_z$ moves away from the centre of mass of the merged system. Conversely, the population losing $L_z$ moves closer to the centre of mass. The result is consistent with the theoretical picture by Huang (1963). Similar orbital decay process works in simulations of gaseous discs (Baruteau, Cuadra & Lin 2011). The angular momentum of merging NSCs, each hosting SMBHs in their centre, is extracted by the stars expanding their orbits and the orbit of the merger remnant shrinks as a backreaction (Fig. 2). Because the SMBHs are embedded in the centre of the remnant, the separation between them decreases as a consequence, facilitating the formation of the SMBHB.

Which stellar particles decelerate the SMBHs? In Fig. 4, we show the origin of stars contributing to decrease $L_z$ of the primary SMBH. We find that the main contributors are the stellar particles initially contained in the NSC hosting the second SMBH (blue dashed). We also find that the second SMBH is mainly decelerated by stars initially belonging to the NSC hosting the primary SMBH. While the stars that initially belong to the NSC hosting the primary SMBH (red dotted) temporarily decelerate the primary SMBH, they actually accelerate it in the end. The contribution, either acceleration or deceleration, may depend on the configuration of the merger, e.g. orbit, BH mass, however, a more detailed study is needed to draw a concrete conclusion.

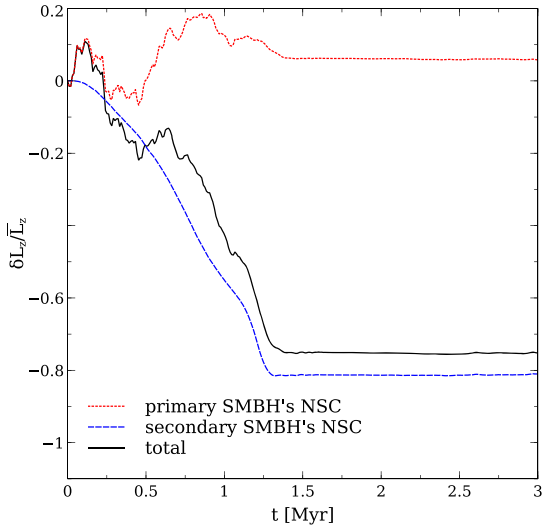


**Figure 4.** Change in $L_z$ of the primary SMBH scaled by $\bar{L}_z$. Red dotted and blue dashed lines are the contribution from stellar particles initially belonging to the NSCs hosting the primary and secondary SMBHs, respectively. Black solid line shows their sum. The primary SMBH is mainly decelerated by stars in the secondary SMBH's NSC.

Motivated by Fig. 4, we study the contribution of stellar particles initially belonging to the NSC of the secondary SMBH in decelerating the primary SMBH in Fig. 5. The upper panel illustrates the distribution of stellar particles reducing $L_z$ of the primary SMBH and shows that the leading arm of the NSC of the second SMBH is located close to the primary SMBH (black circle). The leading arm consists of particles initially on the downstream side. Looking at the right-hand panels of Fig. 2, they are decelerated by their own NSC core, i.e. secondary SMBH and central stars, at the beginning of the merger event and fall to the potential minimum of the entire system. The lower panel shows that the primary SMBH is decelerated by these stellar particles and its $L_z$ is reduced. While Fig. 5 presents only the deceleration of the primary SMBH by stars initially belonging to the NSC of the secondary SMBH, we also find that stars initially belonging to the NSC of the primary SMBH decelerate the secondary SMBH in the same way.

We have shown that the ouroboros effect plays a key role in driving the rapid orbital decay of the SMBHs in merging NSCs. The origin of the ouroboros effect is summarized as follows: (i) At the beginning of a merger event between two NSCs, stars on the downstream (upstream) side are decelerated (accelerated) by the central part of their NSC, including the SMBH, and fall towards (move apart from) the centre of the entire system. (ii) Then, the downstream stars get close to the SMBH embedded in the other NSC and decelerate it. The time-scale of the orbital decay driven by the ouroboros effect would be comparable to the orbital period of the NSC merger since it is triggered by the merger of the NSCs. The orbital decay time-scale by dynamical friction is $\mathcal{O}(\tau_{\rm orb} M_{\rm nsc}/M_2)$ where $\tau_{\rm orb}$ is the orbital time-scale of the second SMBH, $M_2$, in the NSC with a mass of $M_{\rm nsc}$. Therefore, the ouroboros effect would be more important when the second SMBH is less massive. We verify this expectation in Section 4.2.

### 4.2 Accelerated orbital decay due to the ouroboros effect

We next study in detail how the ouroboros effect accelerates the orbital decay of SMBHs embedded in the centres of merging NSCs.

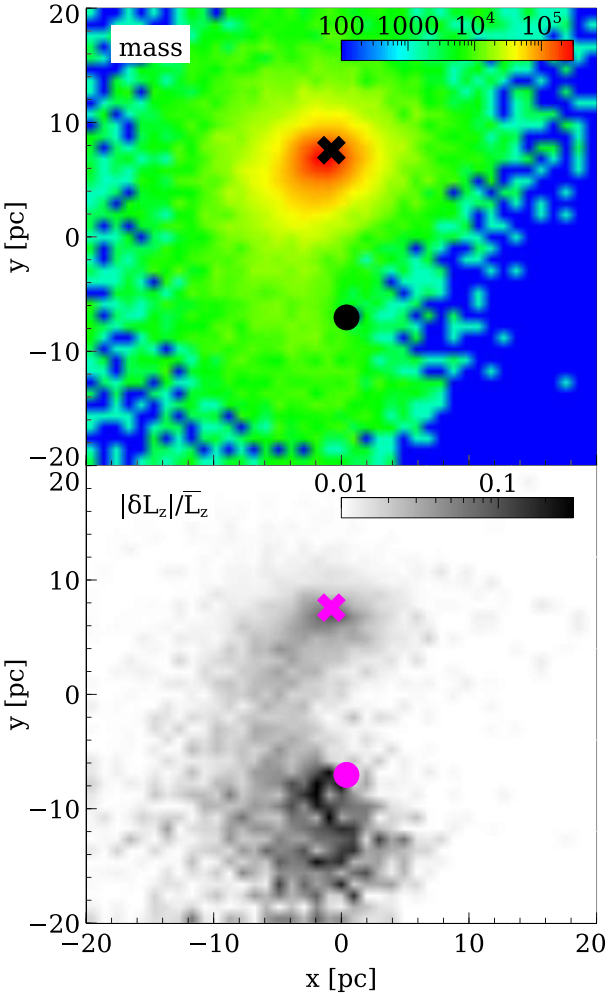


**Figure 5.** Distribution of stellar particles that initially belong to the NSC hosting the secondary SMBH and reduce $L_z$ of the primary SMBH, projected on the *XY*-plane. The contribution in changing $L_z$ of the primary SMBH by the stellar particles is estimated by integrating 51 snapshots up to $t = 0.5$ Myr with the fixed time interval of $\Delta t = 0.01$ Myr. Stellar particles in the range of $Z = [-10{:}\ 10]$ pc at $t = 0.5$ Myr are taken into account. The origin corresponds to the centre of mass of the entire system in the type-M simulation of $q = 0.1$, $d_i = 20$ pc, and $\eta = 1.0$. A circle and a cross represent primary and secondary SMBHs, respectively. (*Upper*) Stellar mass distribution. The colour bar presents stellar mass contained in each pixel (in $M_\odot$). (*Lower*) Contribution in reducing $L_z$ of the primary SMBH, scaled by $\bar{L}_z$. The angular momentum of the primary SMBH is significantly reduced by the leading arm which consists of stars that initially belong to the NSC of the secondary SMBH.

In the top panels of Fig. 6, we present the separation between the SMBHs as a function of time, $d(t)$. The orbital evolution depends on the simulation type (M or O) as well as the mass ratio between the SMBHs, $q$. It is clear that the merger of the NSCs accelerates the orbital decay, especially in the cases of low $q$ in which classical dynamical friction works inefficiently (Chandrasekhar 1943). The middle and bottom panels show the eccentricity and semimajor axis evolution of the SMBHB in each simulation, taking only the two SMBHs into account for computing eccentricity, $e$, and semimajor axis, $a$, i.e. neglecting the gravity of the stellar particles. Because of this assumption, there are a few caveats regarding the evolution of the eccentricity and semimajor axis shown in the middle and bottom panels of Fig. 6 before the SMBHs form a hard binary, i.e. the time while the coloured lines are above the horizontal dashed lines in the top panels. Note that $e$ and $a$ are in fact not defined before the SMBHs are brought close enough. In particular, before the formation of a hard binary, the stellar potential, which we neglect in the definition of $e$ and $a$, contributes to the orbit. Once the hard binary is formed, the stellar potential can be assumed to be constant on the scales of the binary. The semimajor axis depends on both the orbital energy and angular momentum of the SMBHB and its smooth evolution (see bottom panels) indicates that the orbital energy and angular momentum evolve smoothly, too. This is an indication that the binary's evolution is governed by the cumulative interactions between SMBHs and stars, not by a single (perhaps artificial) violent interaction. The latter is unexpected since stars are much less massive than SMBHs and the amount of energy and angular momentum a single star can expel from the SMBHB is limited. Therefore, the binary's dynamical evolution is properly resolved in the simulations. Cyan lines in the central panels show that these simulation results are insensitive to the number of stellar particles.

The result that the orbital decay in our simulations is insensitive to the number of stellar particles, $N_*$, is qualitatively consistent with previous work studying the orbital decay of SMBHBs in merging galaxies or galactic nuclei (Preto et al. 2011; Gualandris et al. 2017, but see also Vasiliev et al. 2015). In spherical systems, the angular momentum and orbital energy of each star are conserved and two-body relaxation is the only mechanism to supply stars to the SMBHB after they are ejected through three-body interactions (re-filling of the loss cone). Since the time-scale of two-body relaxation depends on $N_*$, the orbital decay of SMBHBs is sensitive to $N_*$ in the simulations (Makino & Funato 2004). On the other hand, systems formed through mergers are not spherical (e.g. Preto et al. 2011; Khan, Holley-Bockelmann & Berczik 2015; Khan et al. 2018b) and the loss cone is efficiently re-filled on a time-scale shorter than the two-body relaxation time and that is independent of $N_*$ (see e.g. Yu 2002, for analytical discussions). Therefore, it is unsurprising that the orbital decay of SMBHBs in such systems is insensitive to $N_*$.

In the type-M simulations, the separation between the SMBHs decreases by a factor of a few orders of magnitude in the first Myr with this efficiency depending on $q$. In the cases of $q = 0.1$ and 1.0, the rapid decay driven by the ouroboros effect stops when $d$ drops below the hard binary separation, $d_{\rm hb}$ (horizontal dashed line). The ouroboros effect thus allows the system to bypass the pre-binary and combined effect phases and directly enter the hard binary phase. The evolutionary track to the hard binary phase in the case of $q = 0.01$ is different from the others. The rapid orbital decay driven by the ouroboros effect stops when $d$ drops below the influence radius of the primary SMBH, $d_{\rm b}$ (horizontal dotted line) that corresponds to the time to form a bound binary and enter the combined effect phase. The large difference in the masses of the SMBHs ($10^4$ and $10^6$ $M_\odot$) leads to the disruption of the central part of the NSC hosting the secondary SMBH because (i) the stars are less bound compared to those in the NSC of the primary SMBH; and (ii) the tidal force of the NSC that contains the primary SMBH is stronger. After the disruption, the secondary SMBH is orbiting in the stellar density field of the merged system – a situation comparable to the set-up of the type-O simulations, and the ouroboros effect cannot work efficiently. The combined effect of dynamical friction and three-body interactions of the SMBHs and stars bring the SMBHB more slowly to the hard binary phase, as shown in previous studies (Milosavljević & Merritt 2001; Merritt 2006). While the orbital decay is less efficient, the separation $d$ still decreases by about two and a half orders of magnitude in ∼10 Myr.

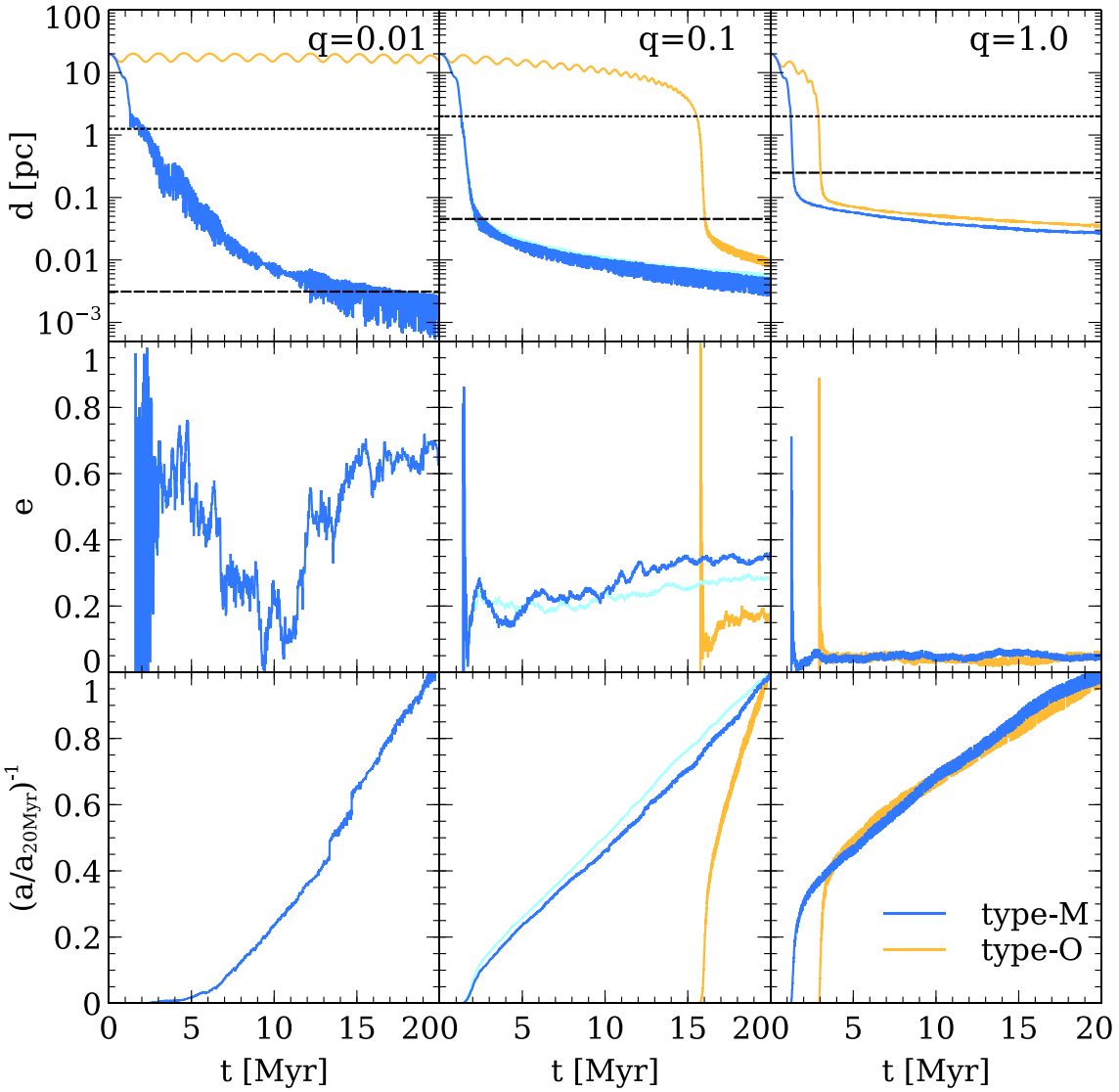


**Figure 6.** Evolution of the relative orbit of the SMBHs. Left-hand, centre, and right-hand panels present the simulation results of $q = 0.01$, 0.1, and 1.0 with the orbital parameters of $d_i = 20$ pc and $\eta = 1.0$. Blue and orange lines represent the results from type-M and -O simulations. (*Top*) Separation between two SMBHs. Dotted and dashed horizontal lines are the gravitational influence radius of the primary SMBH, $d_b$, and hard binary separation, $d_{hb}$, estimated with the mass profiles of the merged system. The mass profiles are derived by stacking and averaging the snapshots in the type-M simulations. (*Middle*) Eccentricity of the orbit of the SMBHB, $e$. (*Bottom*) Inverse semimajor axis of the SMBHB, $1/a$, normalized by that at $t = 20$ Myr. In computing $e$ and $a$, only the two SMBHs are taken into account, i.e. stellar particles are neglected. Cyan lines in the central panels show the results from the M-type simulation with a double number of stellar particles (for the same total stellar mass). The ouroborus effect, active in the type-M simulations but not in the type-O simulations, is responsible for the much faster orbital decay and formation of a hard binary.

After entering the hard binary phase, the orbital decay is less efficient in the type-M simulations with higher $q$. This is simply because at fixed specific angular momentum, the larger the SMBH masses the larger the absolute energy and angular momentum of the binary, and the more energy and angular momentum have to be removed from the SMBHs by the stars. Since stars increase their velocity as a backreaction of the SMBHB orbital decay, they get ejected as the SMBHB shrinks. Eventually, the stars interacting with the SMBHB dwindle because a larger stellar mass is expelled from the centre. This leads to a lower central density of the merged system and lower efficiency of orbital decay in the simulations with larger SMBH masses. This process is generally referred to as core scouring and is the mechanism advocated for creating shallow stellar density profiles, viz. cores, in large elliptical galaxies (cf. Faber et al. 1997; Merritt 2006; Thomas et al. 2016; Rantala et al. 2018, and references therein).

In the type-M simulation with $q = 0.01$, the SMBHB orbit becomes more circular (i.e. $e$ decreases) during the combined effect phase (at $t \lesssim 10$ Myr). This corresponds to orbit circularization by dynamical friction. Note that it is also possible to keep or even increase $e$ with dynamical friction, depending on the density and velocity structure of the system (Tsuchiya & Shimada 2000). In the hard binary phase, $e$ gradually increases with time as predicted by the theoretical model for this phase (e.g. Sesana & Khan 2015) and the resultant $e$ depends on $q$. A dedicated study with longer integration time would be needed to make more concrete conclusions regarding the $e$ evolution.

### 4.3 Dependence of orbital decay times on orbital parameters

To study the dependence of the orbital decay of the SMBHs on the initial merger orbit, we vary the orbital parameters, $d_{\rm i}$ and $\eta$, while fixing $q$ between the two SMBHs, and focusing on type-M models. In the simulations presented in Section 4.2, the orbital parameters are fixed while $q$ and the configuration of the simulations are varied. Therefore, the simulations in this subsection (type-M simulations of $q = 0.1$ in Table 1) are complementary to them.

In Fig. 7, we show the results from type-M simulations varying the orbital parameters, the initial separation between the SMBHs, $d_{\rm i}$, and the parameter controlling the initial angular momentum of the merger orbit, $\eta$, while fixing $q = 0.1$. The top panel shows that the time to achieve the hard binary phase strongly depends on the orbital parameters. When the merging orbit has a smaller orbital energy (viz. smaller $d_{\rm i}$) or smaller angular momentum (viz. smaller $\eta$), the SMBHB enters the hard binary phase in a shorter time, since the orbital energy and angular momentum to be lost are smaller. We also found that in the type-O simulations with identical orbital parameters, the SMBHs take longer to enter the hard binary phase, $\sim$5 and $>$20 Myr in the cases of $d_{\rm i} = 20$ pc and $\eta = 0.5$ and $d_{\rm i} = 50$ pc and $\eta = 1.0$, respectively (results are not shown in the figure), meaning that the ouroborus effect accelerates the orbital decay in all simulations in Fig. 7. The eccentricity evolution (middle panel) depends on the orbital parameters, especially $\eta$ that controls the initial angular momentum of the merging orbit. The SMBHB can have a higher eccentricity when the initial merging orbit is already more eccentric (i.e. smaller $\eta$). The semimajor axis smoothly decreases (bottom panels) and the SMBHB orbital evolution is properly resolved.

## 5 TIME-SCALES OF COALESCENCE FOR SMBHS IN MERGING NSCS

Here, we estimate the time-scale of an SMBHB coalescence based on our simulation results. Plotting the orbital evolution of the SMBHB on a log–log scale, we find an interesting feature after the SMBHB enters the hard binary phase. As depicted in Fig. 8, the SMBHB orbit continues to shrink in a single power-law fashion. The power-law orbital decay is found in all type-M simulations performed in this study. We fit it with a single power-law function after the separation between the SMBH drops below $d_{\rm hb}$ for the first time. The fitting parameters are derived using the least-squares method.

By extrapolating the fitting results, we can discuss the time-scales of SMBH coalescence all the way through to the final GW emission phase. Previous studies have developed a theoretical framework for the dynamical evolution of SMBHBs in the hard binary phase (e.g. Quinlan 1996; Yu 2002; Sesana, Haardt & Madau 2006, 2008) and discussed interesting astrophysical phenomena, including GW emission and hypervelocity stars originated by SMBHBs (Yu & Tremaine 2003; Sesana, Haardt & Madau 2007). They found that the decay of SMBHBs in the hard binary phase is described as

$$\frac{\rm d}{{\rm d}t}\left(\frac{1}{a}\right) = \frac{GH\rho}{\sigma}, \tag{10}$$

where $a$, $\rho$, and $\sigma$ are the semimajor axis of the SMBHB, mass density, and velocity dispersion of stars, respectively. The dimensionless parameter, $H$, is referred to as the binary hardening rate and depends on $a$, $e$, $q$, and the density structure of background stars. Sesana (2010) showed the power-law decay of the SMBHB orbit when $H$ is independent of $a$. In our simulations, the stellar density of the merged system at small radii is higher than Sesana (2010)

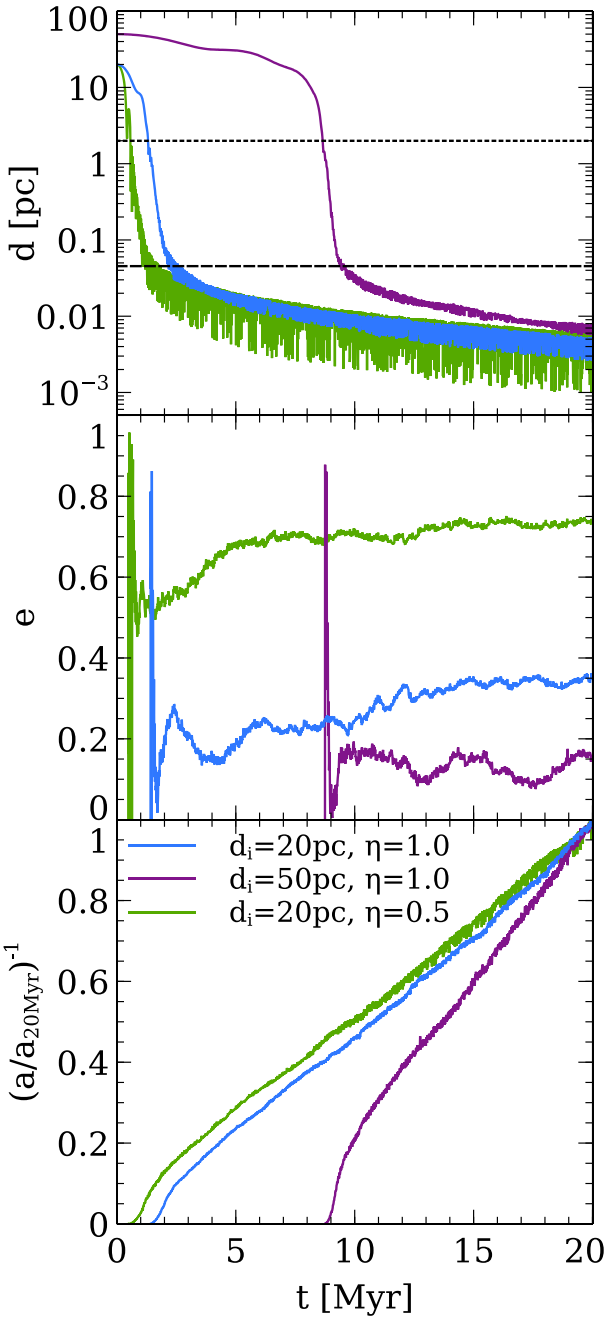


**Figure 7.** Evolution of the relative orbit of the SMBHs in the M-type simulations of $q = 0.1$, varying the two orbital parameters. The adopted orbital parameters are indicated in the legend. (*Top*) Separation between two SMBHs. Dotted and dashed horizontal lines are the gravitational influence radius of the primary SMBH, $d_{\rm b}$, and hard binary separation, $d_{\rm hb}$, estimated with the mass profiles of the merged system. The mass profiles are derived by stacking and averaging the snapshots in the type-M simulations. The estimated $d_{\rm b}$ and $d_{\rm hb}$ are almost independent of the orbital parameters. (*Middle*) Eccentricity of the orbit of the SMBHB, $e$. (*Bottom*) Inverse semimajor axis of the SMBHB, $1/a$, normalized by that at $t = 20$ Myr. In computing $e$ and $a$, only the two SMBHs are taken into account, i.e. stellar particles are neglected. The ouroborus effect accelerates the orbital decay even for significantly different orbital parameters.

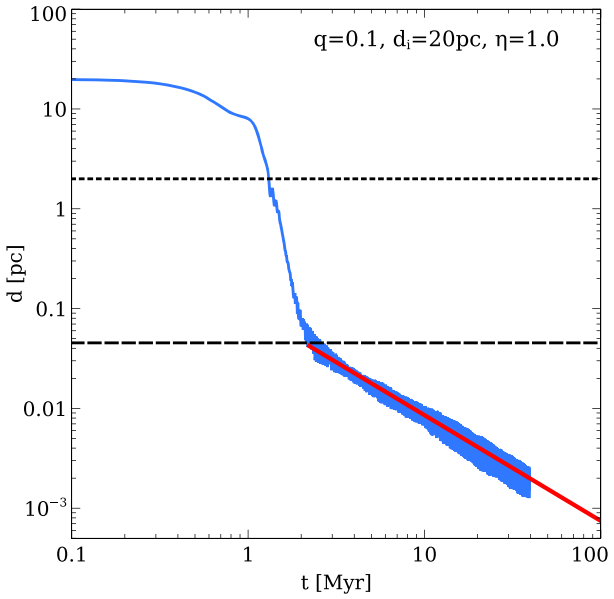


**Figure 8.** Evolution of the relative orbit of the SMBHs in the type-M simulation of $q = 0.1$, $d_i = 20$ pc, and $\eta = 1.0$ (blue) on a log–log scale (the simulation is extended to $t \approx 40$ Myr). Dotted and dashed horizontal lines represent $d_b$ and $d_{hb}$, respectively. In the hard binary phase, the orbital decay of the SMBHB is modelled with a power law and the fitting result is shown as a red solid line.

assumed, and the power-law slope of the orbital decay at $0.1 \lesssim d/d_{hb} < 1$ is explained by $H \propto \rho^{-1/2}$ (i.e. lower $H$ at smaller $a$). Assuming a constant $H$, the orbital decay would be faster than we find.

Let us thus finally estimate the time-scale for SMBH coalescence, $t_{coa}$, in type-M simulations. After entering the hard binary phase, we suppose that initially the decay is driven by stellar hardening, with a power-law decay fit from the simulation down to the scales below which GW emission dominates, for which we adopt the analytical expressions in Peters (1964), fixing the eccentricity of the SMBHB, $e'$. The transition between the two regimes occurs at the semimajor axis $a' = d(t_{pow})$ where the sum of $t_{pow}$ and $t_{GW}$ is minimized (see Table 2 for their definitions).

The time-scales as well as $e'$ and $a'$ are listed in Table 2. We find that the time-scale of SMBH coalescence primarily depends on the mass ratio between two SMBHs, $q$, while the dependencies on the orbital parameters and assumed eccentricity are subdominant. Importantly, $t_{coa}$ is much shorter than the Hubble time in models with $q = 0.01$ and 0.1, and for $q = 1.0$, $t_{coa}$ is about 5 Gyr. Therefore, mergers between NSCs hosting an SMBH in each centre are promising sites of GW emission and exciting targets for upcoming observations.

## 6 SUMMARY AND CONCLUSIONS

The coalescence of SMBHs is one of the most interesting targets for upcoming GW observations. In this paper, we investigate a possible path to accelerate the coalescence of SMBHs due to the presence of host NSCs, bypassing the final parsec problem. We find that an interplay of traditional dynamical friction, stellar hardening, and an extra deceleration force – that we term the 'ouroboros effect' – play a role to decrease the SMBHB's orbit, allowing it to coalesce in less than a Hubble time. This effect is a result of the tidal disruption of the NSCs surrounding the SMBHs, a process which exerts a braking force on to the SMBHB. Because of the scale-free nature of gravity, the ouroboros effect must work not only on the NSC scale but also on larger galactic scales. Interestingly, rapid orbital decay in the first few periods was also reported to occur in mergers between star clusters (Arca-Sedda & Gualandris 2018) and between galactic nuclei (Khan et al. 2016; Khan, Berczik & Just 2018a). It could plausibly be driven by the same mechanism. In Table 3, we list the relevant processes in each phase that the SMBHs experience before their eventual coalescence. The extra deceleration force is most pronounced when the second SMBH is less massive, since dynamical friction becomes less effective in making a binary. When the mass ratio of the binary is close to unity, a hard binary is directly formed within a few periods of the initial merging orbital time.

The extra deceleration force is caused by stars that initially belong to the NSC of the other SMBH. Stars initially on the downstream side tend to lose angular momentum because they are pulled back by their own NSC core, including the SMBH, while stars initially on the upstream side gain angular momentum because they are pulled forward by the NSC core and downstream stars. The exchange of

**Table 2.** Expected time of SMBH coalescence in the merged NSCs (i.e. type-M simulations). Description of each column: (1) Simulation parameters. In the 'HR' run, the number of particles is doubled compared to the fiducial one. (2) Assumed eccentricity. (3) Semimajor axis of the SMBHB to have the minimum coalescence time. (4) Time to drop to $a'$ by the power-law stellar hardening. (5) Time to lose orbital energy of the SMBHB by GW emission. (6) SMBH coalescence time measuring from the beginning of the NSC merger, i.e. $t_{coa} \equiv t_{pow} + t_{GW}$.

| (1) $[q, d_i, \eta]$ | (2) $e'$ | (3) $a'$ (pc) | (4) $t_{pow}$ (Myr) | (5) $t_{GW}$ (Myr) | (6) $t_{coa}$ (Myr) |
|---|---|---|---|---|---|
| [0.01, 20, 1.0] | 0.7 | $2.3 \times 10^{-4}$ | 51.4 | 6.1 | 57.6 |
| | 0.0 | $1.1 \times 10^{-4}$ | 73.2 | 8.8 | 82.0 |
| [0.1, 20, 1.0] | 0.3 | $3.6 \times 10^{-4}$ | 201.4 | 47.5 | 248.9 |
| | 0.0 | $3.2 \times 10^{-4}$ | 224.7 | 53.0 | 277.8 |
| [0.1, 20, 1.0] (HR) | 0.3 | $3.8 \times 10^{-4}$ | 254.2 | 64.3 | 318.5 |
| | 0.0 | $3.4 \times 10^{-4}$ | 285.5 | 72.2 | 357.6 |
| [1.0, 20, 1.0] | 0.05 | $1.5 \times 10^{-3}$ | 3585.0 | 1627.4 | 5212.4 |
| | 0.0 | $1.5 \times 10^{-3}$ | 3602.9 | 1636.2 | 5239.1 |
| [0.1, 50, 1.0] | 0.15 | $2.2 \times 10^{-4}$ | 93.1 | 10.8 | 103.9 |
| | 0.0 | $2.1 \times 10^{-4}$ | 94.5 | 10.9 | 105.5 |
| [0.1, 20, 0.5] | 0.75 | $7.7 \times 10^{-4}$ | 131.1 | 37.2 | 168.3 |
| | 0.0 | $3.6 \times 10^{-4}$ | 312.5 | 88.6 | 401.1 |

**Table 3.** Relevant processes shrinking the orbit of SMBHs in each phase. DF, SH, OE, and GW stand for dynamical friction, stellar hardening, ouroboros effect, and GW emission, respectively. Type-M and -O represent the initial configuration, same as the simulation setup.

| Phase | Type-M | Type-O |
|---|---|---|
| Pre-binary | DF+OE | DF |
| Combined effect | DF+SH+OE | DF+SH |
| Hard binary | SH | SH |
| GW emission | GW(+SH) | GW(+SH) |

angular momentum and orbital energy lets the former fall towards the potential minimum of the merged system and the latter move away from it. Then stars initially on the downstream side strongly decelerate the other NSC.

We find that the orbital decay of the SMBHBs is well modelled with a single power-law function during the hard binary phase, and the power-law slope, i.e. the efficiency of the orbital decay, mainly depends on the mass ratio between the two SMBHs. The decay slope we found is shallower (i.e. slower orbital decay) than that predicted by the theoretical model developed by previous studies. Note that the density and velocity structure of the merged system would be different from those assumed in the previous studies and higher resolution simulations are desirable to discuss the evolution of the SMBHB in the hard binary phase in more detail. Therefore, we leave the direct comparison between simulations and the theoretical model for future studies. We estimated the time-scale of SMBH coalescence based on the extrapolation of the power-law function and find that SMBHs with a mass ratio of 1:10 or 1:100 would emit GWs and coalesce within $\sim$100 Myr from the beginning of the NSC merger while for the equal-mass case the total time is longer, 5 Gyr, but still less than the age of the Universe.

While some more factors, e.g. galaxy merger rate, formation rate of NSCs, time-scale of NSC approach after a galaxy merger and fraction of nucleated galaxies, must be taken into account to make predictions for observations, our estimation would be a positive implication for the future GW observations of low frequencies, such as the LISA, and point to the importance of nucleated galaxies in the low-mass regime.

Our investigations also open other avenues of exploration. For instance, if stars in NSCs are mass segregated and heavier stars tend to sink in the centre of the cluster, the efficiency of stellar hardening may be enhanced by having heavy stars tightly bound to the central SMBHs. Another line of research relates to hypervelocity stars: ejection of stars during the hard binary phase from the large supply of the merged NSC would be a signature of this process and can explain the detection of hypervelocity stars from external galaxies (Erkal et al. 2019).

## ACKNOWLEDGEMENTS

We are grateful to the developers of NBODY6++GPU for making their code publicly available, and thank Saavik Ford, Alessandra Mastrobuono-Battisti, Nadine Neumayer, Mathias Schultheis, and Scott Tremaine for fruitful discussions. We acknowledge helpful comments from the anonymous referee and Manuel Arca-Sedda. GO and OH acknowledge funding from the European Research Council (ERC) under the European Union's Horizon 2020 research and innovation programme (grant agreement No. 679145, project 'COSMO-SIMS'). The Flatiron Institute is supported by the Simons Foundation.

## REFERENCES

Aarseth S. J., 2003, Gravitational N-Body Simulations. Cambridge Univ. Press, Cambridge
Abbott B. P. et al., 2016, Phys. Rev. Lett., 116, 061102
Ahmad A., Cohen L., 1973, J. Comput. Phys., 12, 389
Amaro-Seoane P. et al., 2017, preprint (arXiv:1702.00786)
Antonini F., Merritt D., 2012, ApJ, 745, 83
Antonini F., Capuzzo-Dolcetta R., Mastrobuono-Battisti A., Merritt D., 2012, ApJ, 750, 111
Arca-Sedda M., Gualandris A., 2018, MNRAS, 477, 4423
Barnes J., Hut P., 1986, Nature, 324, 446
Baruteau C., Cuadra J., Lin D. N. C., 2011, ApJ, 726, 28
Begelman M. C., Blandford R. D., Rees M. J., 1980, Nature, 287, 307
Berczik P., Merritt D., Spurzem R., Bischof H.-P., 2006, ApJ, 642, L21
Biava N., Colpi M., Capelo P. R., Bonetti M., Volonteri M., Tamfal T., Mayer L., Sesana A., 2019, MNRAS, 487, 4985
Bonetti M., Haardt F., Sesana A., Barausse E., 2018, MNRAS, 477, 3910
Chandrasekhar S., 1943, ApJ, 97, 255
Chatzopoulos S., Fritz T. K., Gerhard O., Gillessen S., Wegg C., Genzel R., Pfuhl O., 2015, MNRAS, 447, 948
Cuadra J., Armitage P. J., Alexander R. D., Begelman M. C., 2009, MNRAS, 393, 1423
Dehnen W., 1993, MNRAS, 265, 250
Eddington A. S., 1916, MNRAS, 76, 572
Erkal D., Boubert D., Gualandris A., Evans N. W., Antonini F., 2019, MNRAS, 483, 2007
Escala A., Larson R. B., Coppi P. S., Mardones D., 2004, ApJ, 607, 765
Escala A., Larson R. B., Coppi P. S., Mardones D., 2005, ApJ, 630, 152
Faber S. M. et al., 1997, AJ, 114, 1771
Fellhauer M., Lin D. N. C., 2007, MNRAS, 375, 604
Fujii M., Funato Y., Makino J., 2006, PASJ, 58, 743
Genzel R., Eisenhauer F., Gillessen S., 2010, Rev. Mod. Phys., 82, 3121
Georgiev I. Y., Böker T., Leigh N., Lützgendorf N., Neumayer N., 2016, MNRAS, 457, 2122
Ghez A. M. et al., 2008, ApJ, 689, 1044
Gillessen S., Eisenhauer F., Trippe S., Alexander T., Genzel R., Martins F., Ott T., 2009, ApJ, 692, 1075
Gualandris A., Read J. I., Dehnen W., Bortolas E., 2017, MNRAS, 464, 2301
Heggie D. C., 2014, preprint (arXiv:1411.4936)
Hénon M. H., 1971, Ap&SS, 14, 151
Huang S. S., 1956, AJ, 61, 49
Huang S.-S., 1963, ApJ, 138, 471
Iwasawa M., Funato Y., Makino J., 2006, ApJ, 651, 1059
Kelley L. Z., Blecha L., Hernquist L., Sesana A., Taylor S. R., 2018, MNRAS, 477, 964
Khan F. M., Holley-Bockelmann K., Berczik P., Just A., 2013, ApJ, 773, 100
Khan F. M., Holley-Bockelmann K., Berczik P., 2015, ApJ, 798, 103
Khan F. M., Fiacconi D., Mayer L., Berczik P., Just A., 2016, ApJ, 828, 73
Khan F. M., Berczik P., Just A., 2018a, A&A, 615, A71
Khan F. M., Capelo P. R., Mayer L., Berczik P., 2018b, ApJ, 868, 97
Kozai Y., 1962, AJ, 67, 591
Kustaanheimo P., Stiefel E., 1965, J. Math. Bd, 218, 27
Lidov M. L., 1962, Planet. Space Sci., 9, 719
Lupi A., Haardt F., Dotti M., Colpi M., 2015, MNRAS, 453, 3437
Makino J., 1991, ApJ, 369, 200
Makino J., Funato Y., 2004, ApJ, 602, 93
Mastrobuono-Battisti A., Perets H. B., Loeb A., 2014, ApJ, 796, 40
McMillan S. L. W., 1986, in Hut P., McMillan S. L. W., eds, Lecture Notes in Physics, Vol. 267, The Use of Supercomputers in Stellar Dynamics. Springer-Verlag, Berlin, p. 156
Merritt D., 2006, ApJ, 648, 976

Merritt D., 2013, Dynamics and Evolution of Galactic Nuclei. Princeton University Press, Princeton
Mikkola S., Aarseth S. J., 1993, Celes. Mech. Dyn. Astron., 57, 439
Milosavljević M., Merritt D., 2001, ApJ, 563, 34
Milosavljević M., Merritt D., 2003, in Centrella J. M., ed., AIP Conf. Ser. Vol. 686, The Astrophysics of Gravitational Wave Sources. Am. Inst. Phys., New York, p. 201
Mingarelli C. M. F. et al., 2017, Nat. Astron., 1, 886
Moody M. S. L., Shi J.-M., Stone J. M., 2019, ApJ, 875, 66
Nguyen D. D. et al., 2018, ApJ, 858, 118
Nitadori K., Aarseth S. J., 2012, MNRAS, 424, 545
Ogiya G., Burkert A., 2016, MNRAS, 457, 2164
Ogiya G., Mori M., Miki Y., Boku T., Nakasato N., 2013, J. Phys.: Conf. Ser., 454, 012014
Ogiya G., van den Bosch F. C., Hahn O., Green S. B., Miller T. B., Burkert A., 2019, MNRAS, 485, 189
Ostriker E. C., 1999, ApJ, 513, 252
Peters P. C., 1964, Phys. Rev., 136, 1224
Plummer H. C., 1911, MNRAS, 71, 460
Power C., Navarro J. F., Jenkins A., Frenk C. S., White S. D. M., Springel V., Stadel J., Quinn T., 2003, MNRAS, 338, 14
Preto M., Berentzen I., Berczik P., Spurzem R., 2011, ApJ, 732, L26
Quinlan G. D., 1996, New A, 1, 35
Rantala A., Johansson P. H., Naab T., Thomas J., Frigo M., 2018, ApJ, 864, 113
Ryu T., Perna R., Haiman Z., Ostriker J. P., Stone N. C., 2018, MNRAS, 473, 3410
Saha P., 2009, MNRAS, 400, 228
Sánchez-Janssen R. et al., 2019, ApJ, 878, 18
Schödel R. et al., 2007, A&A, 469, 125
Sesana A., 2010, ApJ, 719, 851
Sesana A., Khan F. M., 2015, MNRAS, 454, L66
Sesana A., Haardt F., Madau P., 2006, ApJ, 651, 392
Sesana A., Haardt F., Madau P., 2007, ApJ, 660, 546
Sesana A., Haardt F., Madau P., 2008, ApJ, 686, 432
Springel V., 2005, MNRAS, 364, 1105
Tagawa H., Umemura M., Gouda N., Yano T., Yamai Y., 2015, MNRAS, 451, 2174
Tanaka T., Haiman Z., 2009, ApJ, 696, 1798
Tanikawa A., Umemura M., 2011, ApJ, 728, L31
Tanikawa A., Yoshikawa K., Okamoto T., Nitadori K., 2012, New A, 17, 82
Thomas J., Ma C.-P., McConnell N. J., Greene J. E., Blakeslee J. P., Janish R., 2016, Nature, 532, 340
Tsuchiya T., Shimada M., 2000, ApJ, 532, 294
van den Bosch F. C., Ogiya G., 2018, MNRAS, 475, 4066
Van Wassenhove S., Capelo P. R., Volonteri M., Dotti M., Bellovary J. M., Mayer L., Governato F., 2014, MNRAS, 439, 474
Vasiliev E., Antonini F., Merritt D., 2015, ApJ, 810, 49
Volonteri M., Perna R., 2005, MNRAS, 358, 913
Wang L., Spurzem R., Aarseth S., Nitadori K., Berczik P., Kouwenhoven M. B. N., Naab T., 2015, MNRAS, 450, 4070
Yu Q., 2002, MNRAS, 331, 935
Yu Q., Tremaine S., 2003, ApJ, 599, 1129

## APPENDIX A: STABILITY OF THE NSC MODEL IN ISOLATION

We test the stability of our NSC models hosting a central SMBH of $10^6\,\mathrm{M}_\odot$ by following the dynamical evolution of the systems in isolation. Fig. A1 depicts the radial density (upper) and mass profiles (lower) of the NSC models and shows that the NSCs reasonably keep their initial configuration at least for 20 Myr which corresponds to $\sim 300\,(370)\tau$ for the model with a stellar mass of $M_{\mathrm{nsc,\,tot}} = 10^7\,(2\times10^7)\,\mathrm{M}_\odot$. The large scatter in the central region ($r \lesssim 0.03$ pc) where the enclosed mass falls below the mass resolution ($\sim 150\,\mathrm{M}_\odot$) is due to Poisson noise. While this seems to imply that our results are not reliable in this radial range because of a lack of particles, the main results are insensitive to the number of particle (see Fig. 6). We also observe that the SMBH settles in the centre of the NSC in the simulations of the NSC models, as expected.

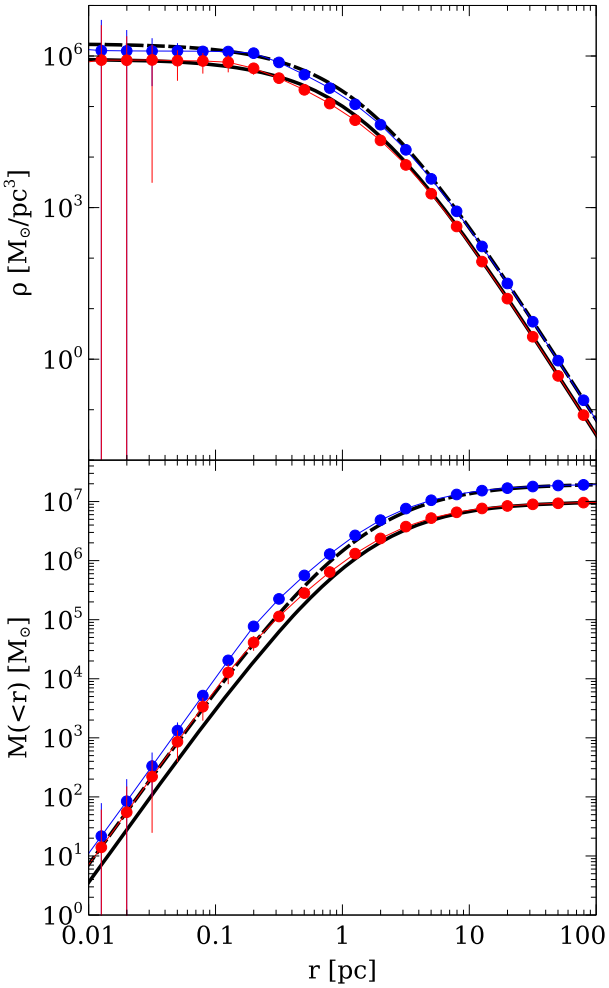


**Figure A1.** Radial profiles of stellar mass density (*upper*) and enclosed stellar mass (*lower*) of the NSC models. Models with a stellar mass of $10^7$ (red) and $2\times10^7\,\mathrm{M}_\odot$ (blue) evolve in isolation for 20 Myr with a central SMBH with a mass of $10^6\,\mathrm{M}_\odot$. Black solid and dashed lines show the analytical expression of the initial configuration of models with a stellar mass of $10^7$ and $2\times10^7\,\mathrm{M}_\odot$, respectively. The origin is taken to be the cluster centre to draw the density profile of the simulated NSCs. In isolation, the NSC models are in a state of dynamical equilibrium.

## APPENDIX B: ACCURACY PARAMETERS

Here, we test the validity of the numerical parameters adopted in our main simulations. Fig. B1 compares the relative energy error, $\mathcal{E}$, in three simulations varying the parameters and finds the energy conservation of the comparable level. Fig. B2 shows the orbital evolution of the SMBHB and we find that our fiducial parameter set (blue) brings the compatible results with those in the simulation

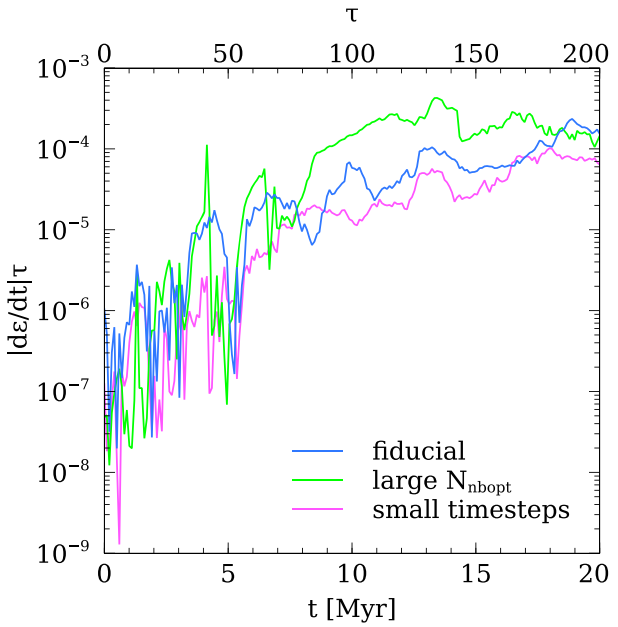


**Figure B1.** Relative energy error, $\mathcal{E}$, originated in one $N$-body time unit, $\tau$, in the type-M model of $q = 0.1$, $d_i = 20$ pc, and $\eta = 1.0$. Blue line presents the result of the simulation with the fiducial parameter set ( $N_{nbopt} = 64$, $\eta_r = \eta_i = 0.005$, and $\eta_u = 0.05$). The simulations of green and pink lines adopt the larger $N_{nbopt} = 550$ ($\eta_r$, $\eta_i$, and $\eta_u$ remain as the fiducial values) and smaller time-steps ($\eta_r = \eta_i = 0.0035$ and $\eta_u = 0.035$) while $N_{nbopt}$ remains as the fiducial value. The level of energy conservation is comparable in the simulations.

of the larger $N_{nbopt}$ (green) and smaller time-steps (pink) while the increase of eccentricity is delayed in them. This does not change our conclusion since the SMBHB coalescence time-scale hardly depends on $e$ (Table 2). Therefore our main simulations have the sufficient accuracy to study the dynamic evolution of the SMBHBs.

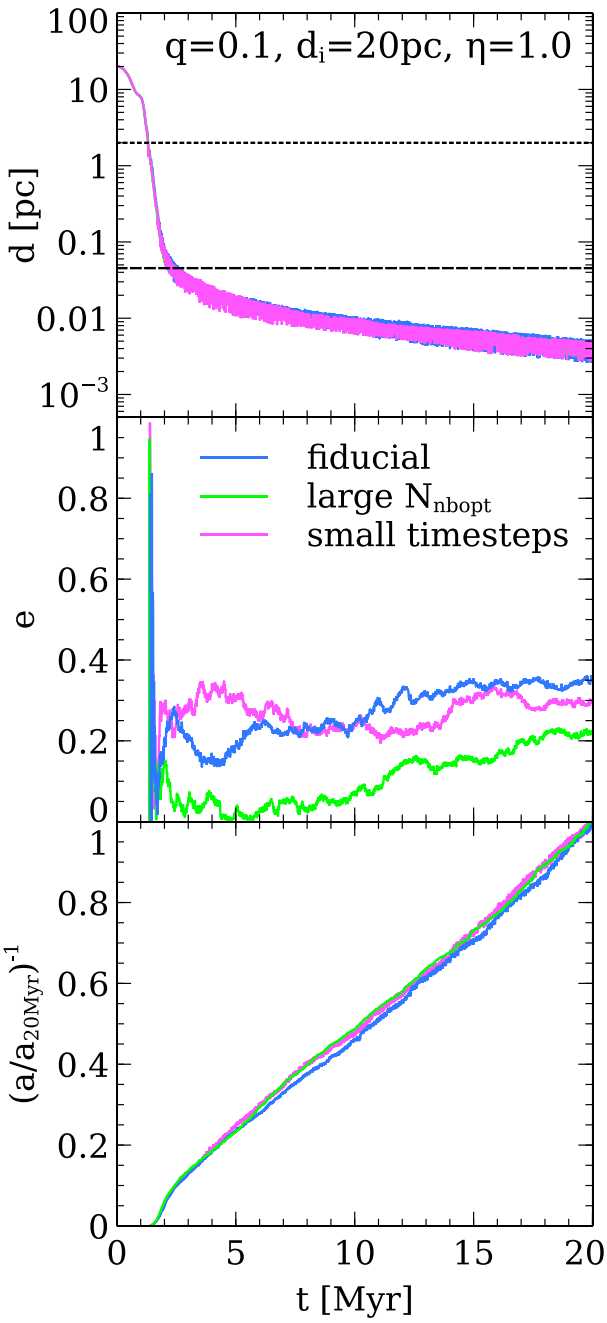


**Figure B2.** Evolution of the relative orbit of the SMBHs in the type-M model of $q = 0.1$, $d_i = 20$ pc, and $\eta = 1.0$. Blue line presents the results of the simulation with the fiducial parameter set ( $N_{nbopt} = 64$, $\eta_r = \eta_i = 0.005$, and $\eta_u = 0.05$). The simulations of green and pink lines adopt the larger $N_{nbopt} = 550$ ($\eta_r$, $\eta_i$, and $\eta_u$ remain as the fiducial values) and smaller time-steps ($\eta_r = \eta_i = 0.0035$ and $\eta_u = 0.035$) while $N_{nbopt}$ remains as the fiducial value. (*Top*) Separation between two SMBHs. Dotted and dashed horizontal lines are the gravitational influence radius of the primary SMBH, $d_b$, and hard binary separation, $d_{hb}$, estimated with the mass profiles of the merged system. The mass profiles are derived by stacking and averaging the snapshots in the simulation of the fiducial parameter set. (*Middle*) Eccentricity of the orbit of the SMBHB, $e$. (*Bottom*) Inverse semimajor axis of the SMBHB, $1/a$, normalized by that at $t = 20$ Myr. In computing $e$ and $a$, only the two SMBHs are taken into account, i.e. stellar particles are neglected. The evolution of the SMBHB is insensitive to the choice of parameters controlling the accuracy of orbital integration and $N_{nbopt}$.

## APPENDIX C: COLLISIONLESS SIMULATIONS

The drag forces that drive the rapid orbital decay of the SMBHs in the first few Myrs of the NSC merger, i.e. the ouroboros effect and dynamical friction, are collisionless processes. Since the number of stellar particles employed in the simulations ($\sim 10^5$) is smaller than that of stars in real NSCs ($\sim 10^7$), collisionality in the simulated systems is higher than in real NSCs. While the orbital evolution of the SMBHB is insensitive to the number of stellar particles in collisional simulations (Fig. 6), we additionally perform a collisionless simulation to address the importance of collisionality in this study. A treecode (Barnes & Hut 1986) accelerated with Graphics Processing Units (Ogiya et al. 2013) is used for this collisionless simulation. To ensure a collisioless nature of the system, the gravitational potential field of particles is softened by introducing the force softening, $\epsilon$, that effectively sets the spatial resolution of the simulations. We employ a Plummer force softening (Plummer 1911) with a softening length $\epsilon = 0.01$ pc, and a cell opening criteria following Springel (2005) with the parameter controlling the force accuracy set to $\alpha = 0.01$. The second-order Leapfrog scheme with the variable time-step (Power et al. 2003) is used for orbit integration.

Fig. C1 compares the orbital evolution of SMBHs in collisonal (blue) and collisionless (brown) simulations. The two simulations show an excellent qualitative agreement before the SMBHs form a hard binary ($d \gtrsim d_{\rm hb}$) and collisional stellar hardening sets in. This result verifies that the drag forces are indeed collisionless processes. Also, Fig. 6 indicates that our main results are insensitive to the possible effect of artificially high collisionality due to the small number of particles. The top panel of Fig. C1 also shows that after the SMBHs form a hard binary, the orbital decay is slower in the collisionless simulation. This is mainly due to the softened gravitational potential field. The separation between the SMBHs is comparable to the force softening, so that the subsequent dynamical evolution in the collisionless simulation is unresolved. On the other hand, the collisional simulation continues to follow the dynamical evolution of the merged system in the framework of the pure Newtonian dynamics since the force softening is not included. Due to the lack of accuracy in force computation and orbit integration, the orbital evolution of the SMBHB in the collisional regime is noisier in the collisionless simulation than in the collisional simulation, as shown in the middle and bottom panels. Therefore, a colissional simulation code is indeed more suited for the purpose of this study even though, of course, there are never enough particles in an *N*-body simulation.

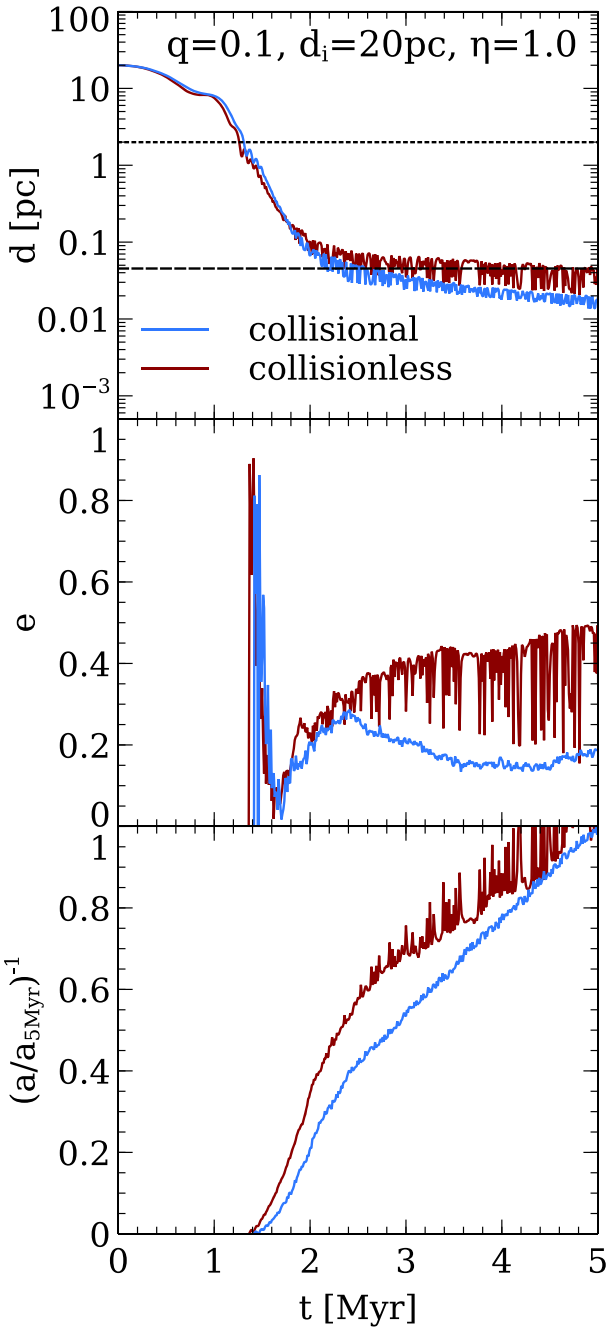


**Figure C1.** Evolution of the relative orbit of the SMBHs in the type-M model of $q = 0.1$, $d_{\rm i} = 20$ pc, and $\eta = 1.0$. Blue and brown lines present the results of simulations using *N*-body codes for collisional and collisionless dynamics, respectively. The same initial condition that consists of two SMBH particles and 131 072 stellar particles (i.e. our fiducial resolution) has been adopted. (*Top*) Separation between two SMBHs. Dotted and dashed horizontal lines are the gravitational influence radius of the primary SMBH, $d_{\rm b}$, and hard binary separation, $d_{\rm hb}$, estimated with the mass profiles of the merged system. The mass profiles are derived by stacking and averaging the snapshots in the collisional simulation. (*Middle*) Eccentricity of the orbit of the SMBHB, *e*. (*Bottom*) Inverse semimajor axis of the SMBHB, $1/a$, normalized by that at $t = 5$ Myr. In computing *e* and *a*, only the two SMBHs are taken into account, i.e. stellar particles are neglected. As expected, the two simulation codes show a good agreement in the collisionless regime, i.e. before entering the hard binary phase ($t \lesssim 2$ Myr).

This paper has been typeset from a TEX/LATEX file prepared by the author.